Journal of Crystal Growth 530 (2020) 125305

Contents lists available at ScienceDirect

Journal of Crystal Growth

journal homepage: www.elsevier.com/locate/jcrysgro

Combination of a millimeter scale reactor and gas chromatography-mass spectrometry for mapping higher order silane formation during monosilane pyrolysis

Guro Marie Wyller[1,*], Thomas J. Preston, Anjitha S.G., Marte O. Skare, Erik S. Marstein

Institute for Energy Technology (IFE), P.O. Box 40, NO-2027 Kjeller, Norway

ARTICLE INFO

Communicated by G.B. Stringfellow

Keywords:
A1. Nucleation
A1. Higher order silanes
A2. Growth from vapor
A2. Fluidized bed reactor
A3. Chemical vapor deposition processes
A3. Polysilicon production processes

ABSTRACT

The formation of higher order silanes during monosilane pyrolysis is studied using a millimeter scale pyrolysis reactor combined with a tailormade gas chromatography–mass spectrometry (GC–MS) setup. We use monosilane diluted in hydrogen and investigate the effects of monosilane inlet concentration (0–100%) and reactor temperature (450–530 °C) on the pyrolysis process. The applied GC–MS technique allows for absolute quantification of mono-, di- and trisilane, as well as relative quantification of higher order silanes with up to eight silicon atoms. We are able to differentiate between higher order silane isomers with up to five silicon atoms and to identify one cyclic silane with six silicon atoms. We find that the outlet concentration of the cyclic silanes as a function of reactor temperature and monosilane inlet concentration have characteristic differences from the outlet concentrations of their non-cyclic counterparts as a function of the same variables. Our data does thereby give experimental evidence for the special role of the cyclic silanes in the pyrolysis process, which has already been pointed to by other authors through numerical and theoretical works. Since cyclic silanes are key species in the particle formation process during monosilane pyrolysis, we hypothesize that avoiding cyclic species can help to reduce fines formation in monosilane pyrolysis reactors. Our detailed mapping of higher order silanes formation gives indications as to which process parameter combinations promote the formation of cyclic silanes and which do not.

1. Introduction

Photovoltaics is one of the fastest growing electricity sources globally, and forecasts predict that it will grow rapidly also in the coming decades [1–3]. Forecasts further predict that the market share of above 90% for silicon based solar cells will stay unchanged [1], indicating that the demand for solar grade silicon will continue to grow.

Purification of silicon for solar cells is an energy demanding process. Up to 40% of the energy needed for the production of a solar panel based on multicrystalline silicon cells is consumed during the preparation and purification of the silicon feedstock [4]. Therefore, finding ways of reducing the energy consumption in these process steps can greatly contribute to the minimization of the cost for solar panels, as well as reducing their carbon footprint and energy payback time. Recent analyses [5] show that reducing the energy consumption for solar grade silicon production by 15–17 kWh/kg_{Si} is, in a CO_2 emission perspective, equivalent to a 1% absolute increase in the energy conversion efficiency for mono- and multicrystalline silicon PV modules. Developments in the silicon purification industry can therefore strongly contribute to making PV an even more environmentally friendly source of electricity.

More than 80% of the polysilicon consumed by the PV industry is produced by pyrolysis of trichlorosilane ($SiHCl_3$) in the Siemens process [1]. Operation of Siemens type reactors is done by numerous silicon producers and the process can give high quality silicon with purity 9–11 N. Even if this technology is considered mature, research (e.g. [6]) is still conducted to optimize it. The energy requirement of the Siemens process is rather high and the one-pass conversion to silicon is low, meaning that recycling of byproducts is necessary.

One way of reducing the overall energy consumption during solar

* Corresponding author at: Department for Solar Energy, Institute for Energy Technology, Norway. Instituttveien 18, 2007 Kjeller, Norway (Visiting address). P.O. Box 40, NO-2027 Kjeller, Norway (Postal address).

E-mail addresses: guro.marie.wyller@ife.no (G.M. Wyller), thomas.preston@ife.no (T.J. Preston), anjitha.geetha@ife.no (S.G. Anjitha), marte.orderud.skare@ife.no (M.O. Skare), erik.stensrud.marstein@ife.no (E.S. Marstein).

[1] www.ife.no.

https://doi.org/10.1016/j.jcrysgro.2019.125305
Received 27 July 2019; Accepted 18 October 2019
Available online 01 November 2019
0022-0248/ © 2019 The Authors. Published by Elsevier B.V. This is an open access article under the CC BY-NC-ND license (http://creativecommons.org/licenses/BY-NC-ND/4.0/).

cell production is to consider replacing the Siemens process by pyrolysis of gaseous monosilane (e.g. [5,7–9]). The production of solar grade silicon by pyrolysis of gaseous monosilane is typically carried out in a fluidized bed reactor (FBR). The FBR has lower energy consumption than the Siemens reactor per kg produced silicon (e.g. [5,7–9]). Moreover, the relatively high chemical yield [9] and the possibility for continuous operation, rather than batch operation as in the Siemens process, makes the FBR process economically feasible.

There are, however, challenges related to formation of dust (often denoted *fines*) during the monosilane pyrolysis process (e.g. [10–13]). Fines formation constitutes a competing chemical pathway to the desired solid silicon production and does therefore cause a reduced yield of solid silicon. Moreover, fines formation leads to challenges related to reactor clogging and reduced material quality (e.g. [11,13]). Overcoming these challenges requires understanding of the chemical complexity hidden in the hundreds of reactions on the way from gaseous monosilane to solid silicon.

With this contribution we bring deeper understanding to the monosilane pyrolysis process by demonstrating a tool for mapping the presence of higher order silanes during the pyrolysis process. Higher order silanes are intermediates on the chemical pathway from monosilane gas to solid silicon particles. Understanding the formation and disappearance of these intermediate species during the pyrolysis process can contribute to increased production yield and improved material quality. This understanding can enable further optimization of industrial monosilane pyrolysis reactors by indicating which reactor parameter combinations promote fines formation and which do not.

2. Theory

Extensive research related to monosilane pyrolysis has been conducted during the past decades. Experimental works ([14–21] and others) as well as modelling works ([12,22–27] and others) have been carried out. Hogness and coworkers [14] were, as early as in 1936, among the first authors to suggest a preliminary chemical reaction mechanism for the pyrolysis of monosilane. Based on their experimental data, they proposed that the reaction is homogeneous and first order. Despite several attempts, these authors were not able to measure disilane in the reaction products. Accordingly, they suggested that the reaction proceeds through two simple steps, sequentially eliminating two hydrogen molecules from monosilane to form solid silicon [14]. The experimental data at which these authors built their model was obtained within the temperature range 380–490 °C and within the pressure range 0.05–0.75 bar. In the view of later research on the topic ([12,17,23,24,28,29] and others) it has become clear that the mechanism suggested by Hogness et al. [14] is too simple to properly describe monosilane pyrolysis. Nevertheless, their work made an important foundation to research in this field, which other researchers have built further upon.

Purnell and Walsh [30] were in 1966 able to measure di- and trisilane as products of monosilane pyrolysis. They developed a more complex mechanism than the one suggested by Hogness et al. [14]. In their mechanism di- and trisilane could also form. In the following years, the mechanism has been continuously expanded and developed to contain an increasing number of species and reactions. In 1987, Yuuki et al. [22] proposed a gaseous reaction model containing 11 elementary reactions and 10 chemical species with up to five silicon atoms. In this model silicon particles were assumed to be created directly from five-membered silicon hydrides. As we have recently demonstrated [31] and will further look into in this contribution, we are able to measure higher order silanes with up to nine silicon atoms during monosilane pyrolysis. Assuming that particles are made directly from five-membered silicon hydrides is therefore clearly too simple.

Giunta et al. [32] and Frenklach et al. [33] developed mechanisms including silanes (saturated silicon hydrides with only single bonds), silenes (silicon hydrides containing silicon-silicon double bonds) and silylenes (radical species, e.g. SiH_3SiH) with up to 10 silicon atoms. In both these mechanisms [32,33], all reactions including species with more than two silicon atoms, were assigned the same reaction coefficients as the analogous reaction with disilane. Later research [28,29,34,35] has identified unequal reaction coefficients for these reactions. Further, these mechanisms [32,33] did not include cyclic species. It has later been shown [23,27,36,37], that cyclic silanes play an important role during monosilane pyrolysis. In this contribution, we give further experimental evidence for the importance of cyclic silanes.

Vepřek and coworkers were, with their series of experimental and theoretical works [36,38–40] on monosilane decomposition during low-pressure plasma conditions, among the first authors to hypothesize the importance of cyclic and more complex three-dimensional structures in the monosilane pyrolysis process [36]. This hypothesis, to which the results presented in our current contribution lend experimental support, has been built further upon by several newer modelling works. Swihart and Girshick [12,23] built on kinetic parameters determined by Ho et al. [41] and on the hypothesis about cyclic silanes proposed by Vepřek et al. [36]. In 1998 these authors published a detailed model of monosilane pyrolysis, containing reversible reactions among species with up to ten silicon atoms and irreversible reactions forming silicon hydrides with 11–20 silicon atoms [23]. Cyclic species were considered in this model in addition to silanes, silenes and silylenes. Like Vepřek et al. [36], Swihart and Girshick proposed that the cyclic species, because of their high stability relative to their non-cyclic counterparts, play an important role in the pyrolysis mechanism.

Several works have taken advantage of the kinetic model proposed by Swihart and Girshick [23] and combined it with other advanced modelling techniques. Girshick et al. [12] coupled it with an aerosol dynamics moment model to predict particle growth, coagulation and transport. Nijhawan et al. [24] further combined it with a flow model and a surface chemistry model developed by Ho et al. [41]. Wong et al. [27] took the mechanisms by Giunta et al. [32] and that by Swihart and Girshick [23] as a starting point and, aided by automated mechanism generation, developed an even more complex mechanism. Based on their modelled results, Wong et al. reported that cyclic structures, especially cyclopentasilane, but also cyclotetrasilane were playing important roles in the formation mechanism. As we shall see later in this contribution, these modeled results are in qualitative agreement with our experimental results.

Other complex modelling works [10,42–44] combine gas phase and surface phase chemical reactions with computational fluid dynamics, particle transport, convection, diffusion, thermophoresis, nucleation and coagulation models to predict particle formation during monosilane pyrolysis. Adamczyk et al. have in several contributions [28,29,34,35,45] applied quantum chemical calculations, statistical thermodynamics, transition state theory and transition state group additivity to determine the Arrhenius parameters of the chemical reactions involved in monosilane pyrolysis.

2.1. Lack of detailed experimental data in the literature

A common theme to many of the works mentioned above is that the modelled results hold an impressive degree of detail, whereas experimental results for model validation are either missing or far less detailed than the modelled results. For example, the detailed models developed in Refs. [12,23,42–44] all lack comparison to experimental data on the formation of higher order silanes during the pyrolysis process. Some newer contributions [10,46,47] compare modelled and experimental results on the effect of operation parameters on monosilane pyrolysis. Even so, there is limited available experimental data compared to the level of detail in the models.

Many of the experimental works in the field of monosilane pyrolysis report macroscopic parameters like *particle formation* [18–20,48], *particle size distribution* and *particle number concentration* [49,50]. These particle-related parameters are the result of thousands of chemical

Fig. 1. Sketch of the horizontal tubular free-space-reactor in which we conduct our monosilane pyrolysis experiments.

reactions. Proper validation of models simulating such macroscopic parameters requires experimental data of not only these macroscopic parameters, but also of the chemical species involved in the reactions. Several authors have reported the appearance of higher order silanes with up to four silicon atoms during monosilane pyrolysis [17,18,51]. Data describing silanes containing more than four silicon atoms during this process is, however, largely non-existent in the literature. The experimental data available in the literature further lack differentiation between isomers with the same number of silicon atoms.

Three main challenges cause the lack of detailed experimental data in the field. First, there has been a lack of reliable measurement techniques to detect and identify higher order silanes and their isomers. Second, the high reactivity of the silanes with oxygen makes them challenging and potentially dangerous to handle. Third, the chemical process itself makes it challenging to detect the intermediate reaction products (i.e. the higher order silanes). Among the chemical steps in the pyrolysis process, the very first step, production of silylene (SiH_2) and hydrogen from monosilane, has one of the highest activation energies [28]. Therefore, under many conditions, as soon as this initial step is overcome, the reaction proceeds quickly to larger and larger species, until eventually, silicon particles are produced. Wu and Flagan [52] used the term *runaway nucleation* to denote this phenomenon.

Our group aims to overcome these three challenges. First, we have in an earlier paper demonstrated the ability to measure higher order silanes with up to eight silicon atoms and differentiating between isomers of silanes with up to five silicon atoms using gas chromatography combined with mass spectrometry (GC–MS) [37]. Second, in the current contribution we apply a millimeter-scale pyrolysis reactor that enables us to map out a complex, multi-dimensional parameter space in an efficient and safe manner: because of its small dimensions, the risks related to explosivity and flammability of the silanes are strongly reduced. Third, in the experiments that we present here, we are controlling the process carefully such that it avoids proceeding all the way to silicon particles. Instead, we are leading higher order silanes, which are process intermediates, out of the reactor and to our GC–MS in which we detect and identify these species.

In this contribution we apply our reactor-GC–MS setup to explore the effects of temperature and monosilane inlet concentration and conduct a mapping of the combined effect of these two parameters on the formation of various higher order silane species. The detailed, isomer specific data that we obtain is a valuable link to modelled data in the field and helps closing the gap in the degree of detail between monosilane pyrolysis models and experimental works regarding monosilane pyrolysis. Specifically, we observe a deviating behavior of the concentration of the cyclic species, as compared to non-cyclic species. This observation gives experimental support to modelled results predicting the stability [23,27,45] of cyclic silanes and a special role of cyclic species during monosilane pyrolysis [23,27,36].

3. Experimental

3.1. Silane reactor

Our monosilane pyrolysis experiments were conducted in a horizontal, tubular free space reactor (FSR), sketched in Fig. 1. The reactor consists of a 124 cm long 1/4“ (6.3 mm) stainless steel 316L pipe with Swagelok fittings in both ends. The inner diameter of the tube is 3.85 mm, giving a reactor volume of only 14.4 cm^3. The temperature of the 80 cm long heated zone is set by the reactor operator and can attain values from room temperature to 600 °C. In the experiment series presented here, we investigate temperatures in the range 450–530 °C. The temperature is continuously measured by six thermocouples placed at different axial positions between the inner metal tube and the insulation material (glass fiber, textile glass braiding and silicone foam tape).

At the temperature settings we used, the absolute difference between the highest and the lowest temperature in the heated zone is about 40 °C, which at a setpoint of 500 °C constitutes a maximum deviation of 5.2% in absolute temperature. Assuming the Arrhenius parameters estimated by Adamczyk et al. [28], the rate of hydrogen elimination from monosilane increases six-fold[2] with a temperature increase from 500 °C to 540 °C. Our temperature uncertainty can, in other words, cause large uncertainties in our results, which we need to be aware of when interpreting our data. The temperature dependence of the formation of higher order silanes is further discussed in Section 4.2.

During an experiment the process gas, monosilane and hydrogen at varied mixing ratios, is led through the reactor. In the experiments presented here, we use a constant total flow of 100 mSLM (standard milliliters per minute), giving a residence time of about 2 s. We vary the monosilane inlet concentration (in volume percent) in the range from 2.5% to 100%. The flow and mixing ratio are controlled by mass flow controllers (MFCs). For monosilane, we use three MFCs of the type Bronkhorst MFC Metal Seal, with flow ranges 0.08–3.8 mSLM, 0.5–25 mSLM and 20–250 mSLM respectively. For hydrogen we use an MFCs of the type Bronkhorst El-Flow Prestige MFC with flow ranges 5–250 mSLM. All the MFCs have rated accuracies of ± (0.1% Rd + 0.5% FS), where Rd represents the actual reading and FS represents the maximum flow of the MFCs. For the flow range we investigated, the largest *relative* uncertainties in the gas flows are within ± 3%. The reactor pressure is controlled by a back-pressure regulator (El-Press, Electronic Back Pressure Controller) with a rated accuracy of ± 0.0175 bar. In the presented experiments, we kept the pressure constant at 1.2 bar. At each combination of reactor temperature and monosilane inlet concentration we inject a sample of the reactor exhaust to the gas chromatograph-mass spectrometer (GC–MS, see Section 3.2). The analysis time of a sample in the GC–MS is approximately 30 min. Therefore, the reactor is always allowed to stabilize for 30 min at each new setting before we sample to the GC–MS.

Depending on the combination of reactor temperature and monosilane inlet concentration, particles might be produced in the reactor (see Sections 4.1 and 5.2). We generally want to avoid reactor settings that cause extensive particle production because particles and other larger species can clog the reactor or the related equipment. We also expect that the presence of particles alters the reaction chemistry. A detailed understanding on the influence of the particles on the reaction chemistry is out of scope for this work; we refer the reader to previous modelling work by Menz and Kraft [25].

Particle production is promoted by increased temperature or monosilane inlet concentration. To minimize the effect of the particles in the reactor, we always scan parameters from lower to higher monosilane inlet concentration or from lower to higher temperature. By

[2] $k(500\ °C) = Ae^{(-Ea/RT)} = 13.6 s^{-1} e^{((-57.3\ kcal/mol)/((1.987 \cdot 10^{-3}\ kcal/mol \cdot K) \cdot 773.15K))} = 8.61 \cdot 10^{-16}\ s^{-1}$ $k(540\ °C) = Ae^{(-Ea/RT)} = 13.6 s^{-1} e^{((-57.3 kcal/mol)/((1.987 \cdot 10^{-3}\ kcal/mol \cdot K) \cdot 813.15K))} = 5.39 \cdot 10^{-15}\ s^{-1}$

scanning this way, we avoid as much as possible that a measurement at one specific reactor setting is influenced by particles made at another reactor setting. After one measurement series, i.e. a series of injections with increased temperature or monosilane inlet concentration until the system clogs or an inlet concentration of 100% monosilane is reached, we open the reactor in both ends and remove particles by blowing through the reactor by pressurized nitrogen. We assume that this procedure brings the reactor back to its initial state, such that new experiments are not influenced by earlier experiments.

3.2. GC–MS

A side stream of the reactor exhaust is led from the reactor outlet to a GC–MS, tailor made for measuring higher order silanes. Our GC–MS system consists of gas chromatograph Agilent 7890B GC and mass spectrometer Agilent 5977A MSD (subtype G7038, quadrupole MS with electron ionization). Readers are referred to our previous work in ref. [37] for a detailed description of the system and its functionality. In this study, we introduce some changes to the system. First, the temperature of the gas handling and loading system is kept at about 120 °C (rather than 60 °C as in ref. [37]). The higher temperature reduces the risk that silanes with a high boiling point condense in the system before they reach the gas-chromatographic columns. We facilitate the temperature increase by replacing electronically controlled valves with pneumatically controlled valves. Second, the injection method presented in ref. [37] is slightly modified: We do not apply the so-called *argon piston* and the *multiposition valve* as described in ref. [37]. Rather we inject by opening a manual valve to the reactor. Since we keep the reactor pressure at 1.2 bar (see Section 3.1), gas will flow into the GC–MS sampling loops which we keep at 1 bar. Our new injection method is simple and it reduces the risk of cross contamination between the samples.

The gas chromatographic system (GC) separates different gasses in time by their varying interaction with the GC columns and, accordingly, their different travelling times through the columns. Different gases and isomers will thus elute to the mass spectrometer (MS) at different times. In the MS, the molecules are bombarded and fragmented by accelerated electrons; we set the acceleration potential to 70 V. Different gas molecules and isomers fragment differently and thus cause different mass spectral patterns. We recently identified and published mass spectra of various higher order silane isomers [37]. Cyclohexasilane (*cyclo*–Si_6H_{12}) is identified [53] based on its boiling point and its elution time of the GC column.

We have calibration standards, provided by Matheson, allowing for an absolute calibration of the signals of mono-, di-, and trisilane. Our most concentrated calibration standard has concentrations of 2%, 0.2% and 0.1% for monosilane, disilane and trisilane respectively. For concentrations higher than these, we calculate measured concentrations by extrapolation. We calculate calibration curves by assuming that the relation between concentration and signal intensity is linear and that zero concentration gives zero signal intensity.

Calibration of species with four or more silicon atoms is not possible at present because we lack reliable calibration standards. We assume that the response factor of every species in the GC–MS is constant as a function of concentration. This assumption implies that the measured signal of a species scales linearly with the concentration of that species. The scaling factors are, however, unknown. When we plot the signals of the higher order silanes semi-logarithmically (see Fig. 2 and Fig. 3), the slope of each plot will be independent of the unknown scaling factors. This way, we can compare the growth rate of the species even if their scaling factors are unknown.

The most abundant m/z in the mass spectrum of trisilane [37,54] is m/z 60. At trisilane concentrations higher than about 0.18%, we get saturation in the signal corresponding to m/z 60. Thus, to increase the dynamic range for trisilane (i.e. the range of trisilane concentrations that we can quantify), we exclude m/z 60 from our quantification of trisilane. Rather, we quantify the trisilane signal by integrating the sum of all measured m/z below m/z 59.5 and above m/z 60.5. When presenting data corresponding to the signals of trisilane and higher order silanes (e.g. in the right panes of Fig. 2 and Fig. 3) we multiply the trisilane signal with a factor equal to the ratio between the full mass spectrum of trisilane and the mass spectrum of trisilane without m/z 60. Introducing this multiplication improves the readability of the figures. The absolute signal intensities as well as the ratio of signals intensities from species with different number of silicon atoms are arbitrary.

The data treatment and data analysis related to the GC–MS measurements are done in the programs Agilent Mass Hunter Qualitative Analysis B.07.00 and Matlab version R2014b.

3.3. Measurement uncertainty

Based on a set of 30 independent measurements of our most concentrated calibration standard, taken over the same period as the measurements presented in this paper, we estimate uncertainties (empirical standard deviations in absolute volume percent) of ± 0.013% for monosilane, ± 0.002% for disilane and ± 0.009% for trisilane. Given the concentrations in this calibration standard (see Section 3.2), we have relative empirical standard deviations below 1% for monosilane, below 1.5% for disilane and below 10% for trisilane. These values give the combined uncertainty of the GC–MS measurement setup itself and the uncertainty of the concentration in the sample injected from the calibration bottle.

The reactor introduces another source of uncertainty to our setup. Based on a set of 12 measurements at equal reactor condition (500 °C and 5% monosilane inlet concentration) taken within one day, we still get relative empirical standard deviations below 1% for monosilane, below 1.5% for disilane and below 10% for trisilane as well as for the higher order silanes present at the given conditions.

When we compare measurements at the same reactor conditions from several days, we observe a day-to-day variation giving a somewhat larger uncertainty, especially for the higher order silanes, of which the absolute concentrations are low. The results shown in Fig. 2 and Fig. 3 are presented such that all data in one pane is taken in one single day. We therefore expect that the relative values of the points within each pane of these figures have relative standard deviations below 10%. In the upper pane of Fig. 2, we have plotted representative standard deviation bars, indicating the magnitude of the day-to-day variation in the monosilane, disilane and trisilane signals.

3.4. Hazards and safety

Monosilane and hydrogen are dangerous to handle. To reduce the risk related to experimentation with these gases, we are using a small reactor with an inner reactor volume of only 14.4 cm^3 (see also Section 3.1). The reactor is placed in a separate room, which is well ventilated and equipped with gas sensors that will automatically shut down the gas supply if monosilane or hydrogen is detected outside the reactor. To further reduce the risk of gas leakage, we pressure test the reactor and all related equipment before each experiment. The equipment is tested at a pressure higher than the pressure of the planned experiment to verify that gas won't leak *out of* the reactor. Further, it is tested at low pressure (about 0.35 bar) to verify that gas won't leak *into* the reactor. The under-pressure test also ensures that no moisture is present in the reactor. The presence of moisture would cause the pressure to rise during an under-pressure test.

All gas lines in our setup are equipped with one-way valves to make sure that hazardous gasses cannot flow backwards into other gas lines in the case of a system failure. For the same reason, we keep the pressure in the silane line lower than the pressure in the other gas lines. Then, even in case of failure in the one-way valves silane will not leak into the other gas lines.

During experimentation, the reactor operator sits in a separate

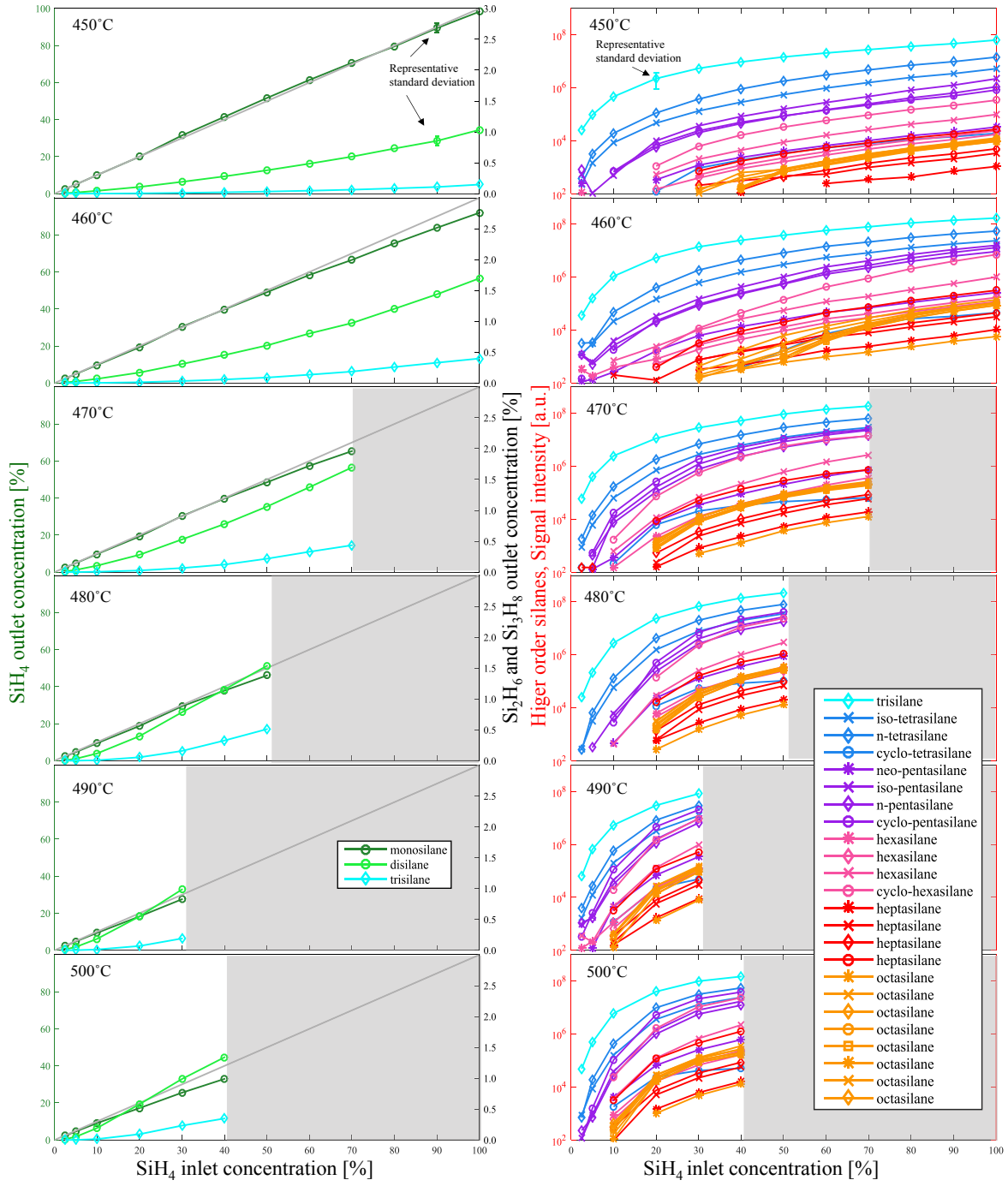

Fig. 2. Outlet concentrations of various silanes as functions of monosilane inlet concentration at different temperatures. Left panes) Absolute output concentrations of monosilane, disilane and trisilane. Right panes) Uncalibrated signals for trisilane and higher order silane isomers. The reactor temperature is indicated in each pane. Grey areas indicate settings that were not tested because of reactor clogging or risk of reactor clogging. The grey diagonal lines in the left panes are guides for the eye and indicate equal inlet and outlet monosilane concentrations. The deviation of the dark-green line from the grey line indicates the extent of reaction. The representative standard deviation bars in the upper panes are calculated from a set of 23 measurements at equal reactor conditions, taken over several different days (see Section 3.3). (For interpretation of the references to colour in this figure legend, the reader is referred to the web version of this article.)

control room from which he or she remotely controls the experimental setup including gas supply, temperature and pressure control and GC–MS measurements. If the operator needs to enter the reactor room during operation, he or she wears fire-proof clothing, ear protection and a face shield.

4. Results

4.1. Formation of higher order silanes as a function of monosilane inlet concentration

Fig. 2 shows outlet signals of monosilane and various higher order silanes as functions of monosilane inlet concentration during monosilane pyrolysis at different reactor temperatures. The left panes of the figure show absolute outlet concentrations of monosilane, disilane and

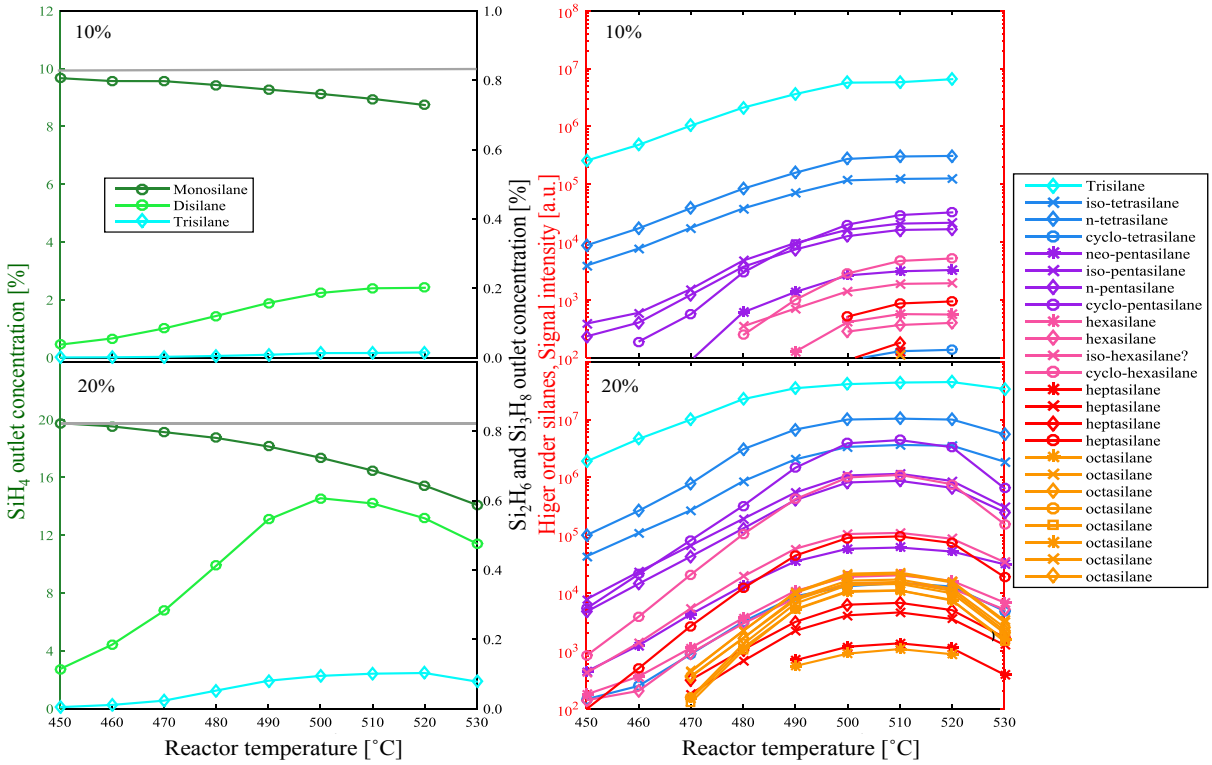

Fig. 3. Outlet concentrations of various silanes as functions of temperature. (Left panes) Absolute output concentrations of mono, di and trisilane. (Right panes) Uncalibrated signals for trisilane and higher order silane isomers. Both panes are plotted as function of reactor temperatures, at monosilane inlet concentrations of 10% (upper panes) and 20% (lower panes). The grey lines in the left panes show equal inlet and outlet monosilane concentrations; deviation of the dark-green line from the grey line indicates the extent of reaction. (For interpretation of the references to colour in this figure legend, the reader is referred to the web version of this article.)

trisilane plotted with a linear axis. The right panes show uncalibrated signals for various higher order silane isomers plotted with a logarithmic axis. Trisilane is included in both panes for clarity and comparison. The reactor temperature is increased from top to bottom of Fig. 2, as indicated by the figure annotations. Grey regions in the plots indicate settings for which production rates of large pyrolysis products or particles are so high that the reactor or parts of the related system clogged, or settings we did not test because we expect clogging. For example, at a reactor temperature of 470 °C, the system clogged at 70% monosilane inlet concentration. Therefore, we did not test concentrations above 70%. At a reactor temperature of 480 °C, the system clogged at 50% monosilane inlet concentration. Therefore, we did not test concentrations above 50%, and so forth. Reactor clogging and the effects leading to it are further discussed in Section 5.2.

We have absolute calibrations only for the signals of mono-, di-, and trisilane, not for the higher order silanes (see Section 3.2). Based on electron capture cross sections for hydrocarbon isomers [55], we assume that species with the same number of silicon atoms have very similar electron capture cross sections and therefore similar MS response factors [37]. Therefore, when studying the results shown in the right panes of Fig. 2, we can directly compare the uncalibrated signals of, for example, two tetrasilane isomers and assume that they give a good indication of the relative concentration of the two isomers. We cannot, however, directly compare the outlet concentration of, for example, a tetrasilane isomer with that of a pentasilane isomer, because these species have different unknown MS response factors (see also Section 3.2).

The grey diagonal lines in the left panes of Fig. 2 indicate zero conversion, i.e. outlet concentration equal to inlet concentration. The conversion of monosilane to other species is in other words represented by the deviation of the dark-green line, indicating the monosilane outlet concentration as measured by the GC analysis, from the grey line, indicating the inlet concentration of monosilane as measured by the MFCs. The green line being higher than the grey line at 450 °C (upper panes of Fig. 2) is unphysical. We believe that this apparent negative conversion of monosilane to other species is explained by the uncertainty related to the GC–MS and the MFCs in our setup (see Sections 3.1 and 3.3).

When comparing the panes corresponding to different temperatures in Fig. 2, one notes an increase in monosilane conversion with temperature. One further notes that the higher the temperature, the higher is the growth rate of the outlet concentrations of di- and trisilane as function of monosilane inlet concentration. The same is the case for the higher order silanes: the higher the reactor temperature, the higher is the growth rate of the outlet concentration of these species as function of monosilane inlet concentration.

Reactor clogging is, in each temperature setting, occurring at similar outlet concentration of higher order silanes. The trisilane signal, for example, is in most of the temperature settings reaching a concentration between 0.3% and 0.4% before the reactor clogs. This level is reached at lower inlet concentration when the reactor temperature is higher.

At 450 °C (upper, right pane of Fig. 2) the signals of the higher order species grow at similar rates as function of inlet concentration, causing parallel lines in the semilogarithmic plot. At 460 °C most lines are still parallel, but the cyclohexasilane (*cyclo*-Si_6H_{12}) signal is growing faster with monosilane inlet concentration than the signals of most of the other species. The cyclopentasilane (*cyclo*-Si_5H_{10}) signal is also increasing faster than the signal of most of the other species. In the data for reactor temperatures of 460 °C and higher, we also notice a remarkable behavior of the cyclotetrasilane (*cyclo*-Si_4H_8) signal. This signal first increases relatively quickly with inlet concentration and then flattens out at higher inlet concentrations. The special behavior of the cyclic higher order silanes is further discussed in Sections 5.1 and 5.4.

4.2. Formation of higher order silanes as a function of reactor temperature

The results in Fig. 2 indicate that the formation of higher order silanes during monosilane pyrolysis varies both with inlet concentration and temperature. To further investigate the effect of reactor temperature on formation of higher order silanes, we conduct experiments in which we keep the monosilane inlet concentration fixed and vary the reactor temperature. Since the reactor history can influence the reaction chemistry, scanning along the temperature dimension does not necessarily give the exact same result as scanning along the concentration dimension.

The results of investigations with fixed concentration and varied temperature are presented in Fig. 3. The upper panes show the result of investigations with 10% monosilane inlet concentration. The lower panes show the result of investigations with 20% monosilane inlet concentration. As in Fig. 2, the left panes show calibrated outlet concentrations of mono-, di-, and trisilane, and the right panes show uncalibrated signals for trisilane and higher order silanes. The left panes are plotted with a linear axis, whereas the right panes are plotted with a logarithmic axis. Some parameter combinations are represented both in Fig. 2 and Fig. 3. Even so, the data are from different measurement series, obtained at different days. As we elaborate in Section 3.3, there can be minor differences between data obtained at different days.

As in Fig. 2, the grey lines in the left panes indicate zero conversion of monosilane. The chemical conversion of monosilane to other species is thus represented by the deviation of the dark-green line, representing the monosilane inlet concentration as measured by the GC analysis, and the grey line, representing the monosilane inlet concentration, as measured by the MFCs.

The monosilane outlet concentration decreases with temperature both at 10% and 20% monosilane inlet concentration (upper and lower pane of Fig. 3). This decrease indicates that the monosilane conversion increases with temperature. The outlet concentrations of all the other species increase with temperature at the lower temperatures. At higher temperatures, they flatten out, reach a maximum, and eventually start to decrease with temperature. The temperature of the maximum outlet concentration depends on the inlet concentration. At 20% monosilane inlet concentration (lower pane of Fig. 3) the maximum of the disilane concentration appears around 500 °C. At 10% monosilane inlet concentration (upper pane of Fig. 3) the disilane outlet concentration seems to flatten out and reach a maximum at around 510 °C or 520 °C. Since our highest measured temperature in this series is 520 °C, our data is inconclusive regarding the exact temperature of the maximum outlet concentration.

The observed behavior with a maximum in outlet concentration of the higher order silanes as function of reactor temperature agrees well with results that we have reported earlier [20,21,31,53] and with results reported by others [17,18,56].

The behavior of the cyclic silanes constitutes a difference between the results at 10% monosilane inlet concentration and 20% monosilane inlet concentration. At 10% monosilane inlet concentration (upper pane of Fig. 3), the cyclopentasilane signal increases slightly faster with temperature than the signals of the other pentasilanes. Similarly, the cyclohexasilane signal increases slightly faster than the signals of the other hexasilanes. At 20% monosilane inlet concentration (lower pane of Fig. 3) this effect is even more pronounced: the cyclopentasilane signal increases considerably faster than the signals of the other pentasilanes and end up at a signal strength which is comparable to that of the tetrasilanes. The cyclohexasilane signal increases considerably faster than the signals of the other hexasilanes and end up at a signal strength which is comparable to that of the non-cyclic pentasilanes. Note, however, that the MS response factors for these species are unknown (see Section 3.2). We can therefore *not* conclude that the *concentration* of cyclopentasilane is comparable to that of the non-cyclic tetrasilanes or that the *concentration* of cyclohexasilane is comparable to that of the non-cyclic pentasilanes.

At the highest temperatures we measure (> 520 °C), the decrease in outlet concentration with temperature is more pronounced for cyclopentasilane than for the other pentasilanes. Similarly, the decrease in outlet concentration with temperature is more pronounced for cyclohexasilane than for the other hexasilanes.

The special behavior of the cyclic silanes compared to that of the non-cyclic ones is in line with the observations discussed in Section 4.1 and also with results that we have published earlier [37] and results published by other groups [23,27,36,57]. These results are further discussed in Sections 5.1 and 5.4.

5. Discussion

5.1. Interlinking of reactor process parameters during monosilane pyrolysis

Many externally controlled parameters influence the formation rates of higher order silane species during monosilane pyrolysis. In addition to temperature and monosilane inlet concentration, which are devoted most attention in this paper, other important parameters include the reactor geometry itself, flow rates, choice of diluent gas, and the presence of silicon particles. These parameters span a multi-dimensional parameter space. Several studies ([17,18,20,21,31,53,56] and others) have investigated the formation of higher order silanes during monosilane pyrolysis and reported a maximum in the concentration of higher order silanes as function of temperature. The temperature at which the highest outlet concentration is observed varies between these studies. This variation can be caused by deviations in any of the parameters spanning the multidimensional parameter space mentioned above. In one of our earlier contributions [31] we studied how *temperature* and *residence time* together influence the formation of higher order silanes during monosilane pyrolysis. In the present contribution we study how *temperature* and *monosilane inlet concentration* together influence this process.

Fig. 4 shows the two-dimensional landscapes for outlet concentrations of disilane (left pane) and trisilane (right pane) as functions of *temperature* and *monosilane inlet concentration*. Fig. 5 shows the same landscapes for selected tetrasilanes, pentasilanes and hexasilanes. These figures are different representations of the data shown in Fig. 2 and Fig. 3. The data collection is the same. Each datapoint in the figures is the result of a GC–MS measurement (see Section 3.2). Along the temperature dimension, there are datapoints at 450 °C, 460 °C and further with intervals of 10 °C in the entire temperature range. Along the concentration dimension, there are datapoints at 2.5%, 5%, 10%, 20% and further with intervals of 10% in the rest of the concentration range. Interpolation between these datapoints is done in graph plotting by Matlab version R2014b.

The outlet concentration in Fig. 4 is shown in volume percent. Since we lack calibration standards for the higher order silanes with more than three silicon atoms (see Section 3.2), the data in Fig. 5 is in arbitrary units. The black lines in Fig. 4 indicate the outer border of the parameter combination space that we were able to measure without being hindered by clogging of the reactor or the related equipment. The hatched area indicates conditions at which no measurement was made either because clogging was anticipated or because of limitations in available laboratory capacity. In Fig. 5 these indications (black line and hatched area) are omitted for increased readability.

We deliberately chose not to conduct measurements at all reactor conditions to avoid severe reactor clogging or permanent damage of related equipment.

Fig. 4 indicates that the highest outlet concentrations of di- and trisilane are found at different reactor conditions. We observe the highest outlet concentration of disilane at 460 °C and 100% monosilane inlet concentration, whereas we observe the highest outlet concentration of trisilane at 480 °C and 50% monosilane inlet concentration. These are the conditions that give the highest outlet concentrations *that we can measure* rather than the overall maximum concentration. Higher

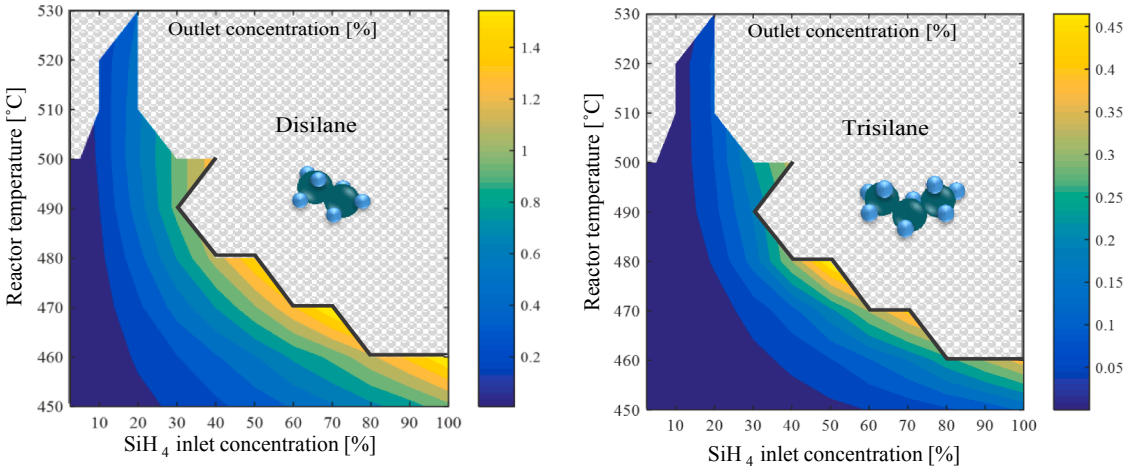

Fig. 4. Map of outlet concentrations of disilane (left pane) and trisilane (right pane) as function of reactor temperature and monosilane inlet concentration. The outlet concentrations are given in volume percent. The black lines indicate the outer border of the parameter combination space that we were able to measure without being hindered by clogging of the reactor or the related equipment.

concentrations than those we report here might be attained at the reactor conditions that we are hindered from exploring due to system clogging.

The higher temperature of the maximum point in our measured trisilane concentration landscape compared to the maximum point in our measured disilane concentration landscape can be related to the fact that trisilane has higher rank than disilane in the monosilane pyrolysis reaction network. The concentration of a certain species in the reactor exhaust results from a balance between the reactions that produce the species and the reactions that consume the species. The differences between the trisilane and disilane concentrations point to subtleties in the balance between the formation and destruction reactions of these species. The present work provides a goalpost for detailed kinetic modelling. Such modelling, however, is outside the scope of our work.

Fig. 5 indicates that we measure the highest signal of all the non-cyclic tetrasilane and pentasilane isomers that we investigate at 480 °C and 50% monosilane inlet concentration. For the non-cyclic hexasilanes

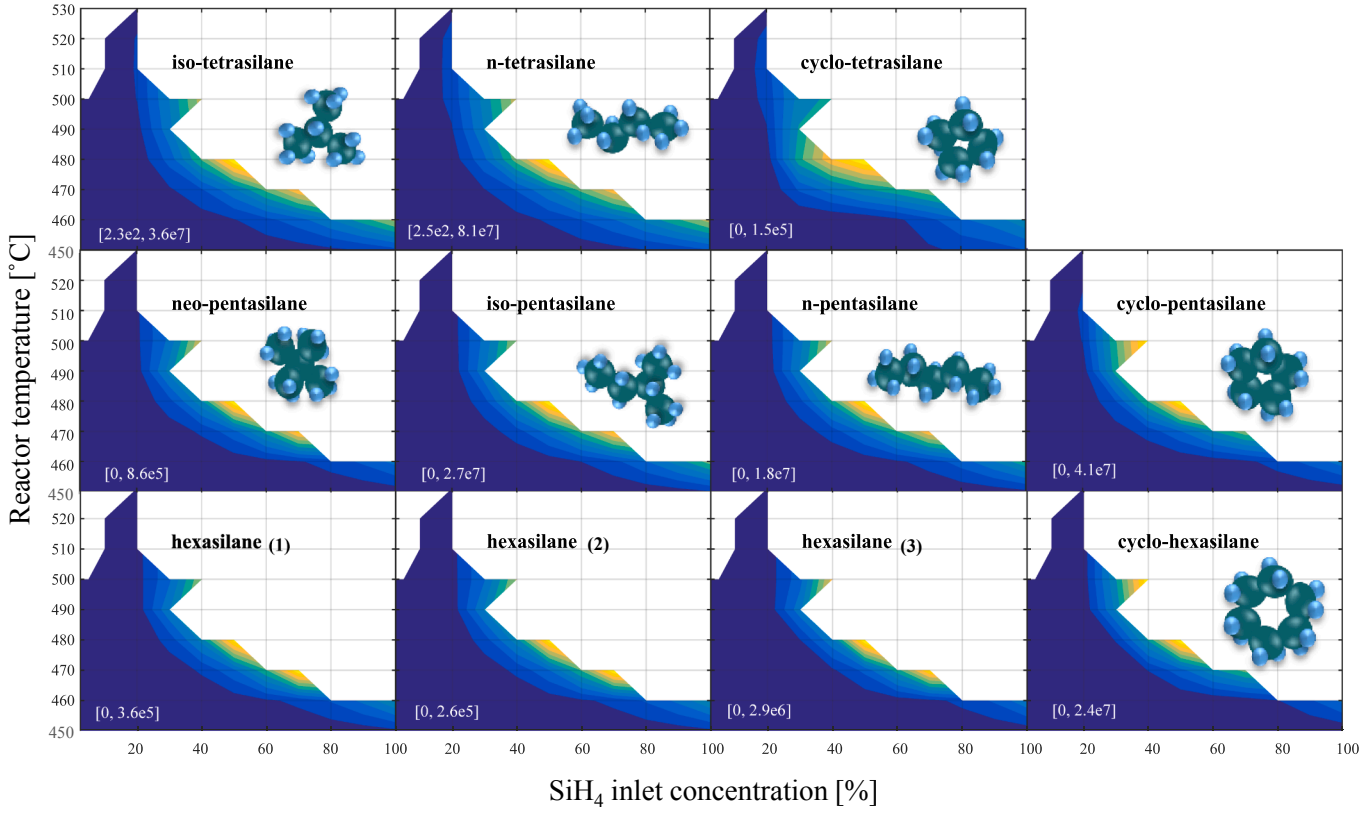

Fig. 5. Map of outlet concentrations (in arbitrary units) of selected tetrasilane, pentasilane and hexasilane isomers as function of reactor temperature and monosilane inlet concentrations. As we haven't yet identified the different non-cyclic hexasilane isomers, we have labeled them with numbers (1, 2, 3). Each isomer is plotted with different linear arbitrary scales, made for optimizing the contrast for that isomer. The numbers printed in white in the lower left corner of each pane indicate the range [lowest value, highest value] of the datapoints in the respective pane.

we measure the highest signal either at 480 °C and 50% monosilane inlet concentration, or at 470 °C and 70% monosilane inlet concentration.

The cyclic silanes follow a different pattern. Cyclopenta- and cyclohexasilane differ from the other species by the high signal attained at 500 °C and 40% monosilane inlet concentration. Cyclotetrasilane show the highest signal at 480 °C and 50% monosilane inlet concentration. As opposed to all the other species we detect, it attains a relatively high value also at 480 °C and 40% monosilane inlet concentration. All the cyclic species have a relatively low signal at 470 °C and 70% monosilane inlet concentration compared to the non-cyclic species.

Summing up the observations in Fig. 5 we see that there is a general tendency for the cyclic species to reach high outlet concentrations at *lower* monosilane inlet concentrations and *higher* temperatures than the non-cyclic species. The *low* monosilane inlet concentration of the maximum point in the measured higher order silane concentration can be explained by the high stability of the cyclic silanes relative to the non-cyclic ones [23,27,45] (see also Section 5.4). Because of this high stability, it will, once formed, be unlikely that a cyclic species decomposes. Relatively high concentrations of cyclic species can therefore build up even at low monosilane inlet concentrations. The *high* temperature of the maximum point in the measured higher order silane concentration can be explained by the high rank of cyclic silanes in the monosilane pyrolysis process. Forming a cyclic silane requires more chemical steps than forming a linear silane with the same number of silicon atoms. The probability of forming a cyclic silane is thus dependent on the rates of several intermediate steps, each of which depend on temperature. The majority of these steps are endothermic, meaning that they will proceed faster at a higher temperature.

As we will explain in more detail in Section 5.4, the cyclic species play a key role in the formation of particles. We therefore hypothesize that if one desires avoiding particle formation through heterogenous nucleation, one should avoid parameter combinations that cause extensive production of cyclic silanes. The maps in Fig. 5 suggest that *low* temperatures and *high* monosilane inlet concentrations are favorable to prevent the concentrations of cyclic species form building up during monosilane pyrolysis.

5.2. Clogging of reactor and related equipment

We would like to emphasize that clogging and the parameter combination at which it happens are not a main result of our research. Rather, it should be considered an unwanted side effect of our experimentation. Nevertheless, the results displayed in Fig. 2, Fig. 4 and Fig. 5 show that there is a general trend that clogging of the system appears at lower silane inlet concentration when the reactor temperature is increased. The experiments conducted at 490 °C and 500 °C run counter to this trend. At 490 °C, the setup clogged already at 40% monosilane inlet concentration, whereas at 500 °C it clogged at 50% monosilane inlet concentration. As of now, we do not know the cause of this deviation from the normal trend with the system clogging at lower concentration when the temperature is increased.

We hypothesize that the clogging mechanism is different at different temperatures. At high temperatures (500 °C and higher) we observe large amounts of particles in the reactor and we assume that the clogging is mainly caused by these solid particles. At lower temperatures, we observe fewer particles. Still, we experience that the system (for example the filters or the pressure regulator, see Fig. 1) is clogging, causing the reactor pressure to rise. We hypothesize that the clogging at these temperatures is caused by higher order silanes with high boiling points, rather than only by solid particles. Silanes with four or more silicon atoms have boiling points above 100 °C [37]. These silanes can therefore easily condense at cold surfaces and cause or contribute to clogging of our system.

5.3. Trends in the formation of higher order silanes

Fig. 2 in Section 4.1 indicates that at a reactor temperature of 450 °C the ratio between the signals of the various higher order silane species are approximately constant over a large range of monosilane inlet concentrations. With few exceptions, for monosilane inlet concentrations in the range from 60% to 100%, the ratio of the *n*-tetrasilane signal to the signal of any of the higher order silanes with 4–7 silicon atoms is constant to within 30%. For higher order silanes with 8 silicon atoms, the same is true to within 40%. This is the case although the *n*-tetrasilane signal is approximately three orders of magnitude stronger than the heptasilane and octasilane signals. At higher reactor temperatures (460 °C and higher, rows 2 through 6 in Fig. 2), the ratios between the signal of the higher order silanes differ more.

Similar results have been discussed by other authors. Vepřek et al. [36] observed a constant ratio among the concentrations of all the higher silanes relative to each other, as well as to monosilane for the entire range of experimental conditions where the authors did not observe nucleation during silane glow discharge at varied current densities. Based on their observations, they suggested that there exists a dynamic equilibrium between the higher order silanes. Swihart and Girshick [23] considered the role of equilibria during monosilane pyrolysis by analyzing monosilane pyrolysis both with kinetic and thermodynamic simulations. Although the overall thermodynamic equilibrium for monosilane pyrolysis in hydrogen is nearly complete conversion to solid, crystalline silicon and gaseous hydrogen, Swihart and Girshick claimed that the kinetics are such that they hinder the system from reaching this overall equilibrium state. Under many conditions, there are kinetic bottlenecks that will limit the nucleation rate, thus hindering the system from reaching equilibrium [23]. They report that for many conditions there is a kinetic bottleneck for growth from higher order silanes containing 7 silicon atoms to higher order silanes containing 8 silicon atoms. In their interpretation [23], evidence for the bottleneck is that all species with seven or fewer silicon atoms are in partial equilibrium with each other.

The nearly constant ratio that we observe between the signals of several higher order silanes at 450 °C appear to be in line with the considerations by Swihart and Girshick [23] and suggests the presence of a kinetic bottleneck to further growth from the species that we observe at this temperature. The fact that we at 450 °C were able to increase the monosilane inlet concentration to 100% without observing reactor clogging (see Section 4.1) supports the theory that some reaction leading to particle formation does not happen or happens only at a very low rate at this temperature. A reaction happening at a low rate compared to other reactions may cause a kinetic bottleneck in the network.

5.4. Trends in the formation and disappearance of cyclic higher order silanes

Several authors (e.g. [23,27,36]) have, mainly through numerical methods, pointed to the importance of cyclic silanes on the pathway to formation of larger silicon clusters or particles during monosilane pyrolysis. The same has been shown for disilane pyrolysis with experimental and numerical methods [57]. In our data, we observe two trends in the formation and disappearance of higher order cyclic silane species. First, the signals of these species *increase* faster than their non-cyclic counterparts as a function of temperature or monosilane inlet concentration (Fig. 2 and Fig. 3). Second, the signals of the same species *decrease* faster at high temperatures (Fig. 3).

The *increase* in the concentration of cyclic silanes can be explained by the stability of cyclic silanes compared to their non-cyclic counterparts [23,27,45] and by the mechanism that has been suggested for the pyrolysis process. Several authors [23,27,36,57] have suggested that the road to cluster formation includes the formation of higher and higher order silanes until a relatively stable, cyclic polysilane is

produced. From this cyclic species the elimination of silylene is unlikely since it requires the simultaneous breaking of two silicon-silicon bonds [23,36]. Once a cyclic silane is formed, it will therefore be relatively unlikely that it decomposes to two separate silicon-containing species. Specifically, it has been predicted [27] that, at reactor conditions of 750 °C and 10% monosilane inlet concentration, cyclopentasilane will be the most abundant of the pentasilane isomers. This prediction, which Wong et al. [27] arrived at through kinetic modelling, is in good qualitative agreement with our experimental results.

The fast *decrease* in the signals of cyclic silanes compared to non-cyclic silanes at higher temperatures (see Fig. 3) suggests that cyclic species are consumed faster than non-cyclic species when particles are formed. The observed decrease tempts us to speculate that cyclic silanes – to a larger degree than non-cyclic silanes – are built into larger three-dimensional, polycyclic structures which form the basis for particle formation. Similar ideas have been suggested by other authors. These authors argue that silylene elimination from a cyclic silanes is unlikely, but that hydrogen, on the other hand, relatively easily can be eliminated from cyclic species [23,36]. Hydrogen elimination will leave a reactive site which can easily react with e.g. silylene [36]. Cyclic species can thus relatively easily grow further into larger three-dimensional species [23,36] forming the basis for particle formation.

Vepřek et al. [36] have reported a sudden decrease in the concentration of higher order silanes at the onset of particle formation in their experiments, similar to what we observe in our data. These authors report that the decrease was most pronounced for tetra- and pentasilane, which were the highest order silanes they were able to detect [36]. Based on their observations, they suggest that higher order silanes were readily consumed by particle formation because these species form the basis for the particles. We are able to measure even higher order silanes than Vepřek et al. [36] and to differentiate between various isomers. We can thus add nuance to their statement by suggesting that especially higher order *cyclic* silanes are strongly consumed by particle formation.

As of now, we have identified cyclic tetrasilane, cyclic pentasilane and cyclic hexasilane in our measurements (see Fig. 2, Fig. 3 and Fig. 5). We have not yet identified the various heptasilane species. Studying the signal development of various species as function of temperature at 20% monosilane inlet concentration (lower right pane of Fig. 3), we notice that one of the heptasilane isomers exhibits a special behavior compared to the other heptasilanes. The signal of this special heptasilane isomer, which is indicated with circular symbols in the plot, develops faster than the other heptasilane signals as a function of temperature and reaches a maximum signal comparable to that of the strongest non-cyclic hexasilane signal. At the highest temperature the decrease with temperature is more pronounced for this signal than for the signals of the non-cyclic hexa- and heptasilanes. This development is very similar to what we observe for cyclopenta- and cyclohexasilane. We therefore speculate that this heptasilane isomer is cyclic. If the identification of the cyclic heptasilane is correct, the special behavior of the cyclic silanes discussed above holds true for cyclic heptasilane in addition to cyclic tetra-, penta- and hexasilane.

6. Conclusion

We have developed a miniature scale monosilane pyrolysis reactor which we use in combination with GC–MS to investigate the formation of various higher order silane species as a function of temperature and monosilane inlet concentration during monosilane pyrolysis. Our results give experimental evidence to the special role of cyclic silanes in the pyrolysis process, which have been pointed to, mainly by numerical and theoretical works, by other authors [23,27,36].

In most of the temperature range we investigate (450–510 °C), we find that the outlet concentrations of cyclic higher order silanes *increase* faster as function of temperature or monosilane inlet concentrations than the outlet concentrations of non-cyclic higher order silanes. At the highest temperatures we investigate (510–530 °C), we find that the outlet concentrations of cyclic higher order silanes *decrease* faster as function of temperature than the outlet concentrations of non-cyclic higher order silanes. We hypothesize that the fast decrease in the concentration at high temperatures appears because cyclic higher order silanes, more than their non-cyclic counterparts, are likely to grow further into larger silicon hydride species and eventually into particles. This hypothesis implies that to reduce particle formation during monosilane pyrolysis one should avoid parameter combinations at which cyclic silanes are produced at high rates.

We realize that the formation and disappearance rates of all the various higher order silane isomers are functions of a large, multi-dimensional parameter space of which we have only explored two dimensions in this work. Nevertheless, our detailed mapping of higher order silanes outlet concentration (see Fig. 5) indicates that at relatively low temperatures (< 470 °C) and high monosilane inlet concentrations (70–100%) monosilane pyrolysis takes place without extensive formation of cyclic higher order silanes. The results presented in this paper thus suggest that low temperatures combined with high monosilane inlet concentration is favorable for avoiding particle formation during monosilane pyrolysis.

Declaration of Competing Interest

The authors declared that there is no conflict of interest.

Acknowledgment

We would like to thank Hallgeir Klette and Anders Steinsland for their guidance and practical help in installing and using lab infrastructure in the Fornylab lab at IFE. We are also grateful for the encouragement from Trygve Mongstad to build the millimeter scale reactor, *Milly*. Further, we would like to thank Cornelis Arnoldussen at IndCon AS for his great help with programming the remote-control system for our reactors and Eivind Utheim and Jon Mathias Hallem at GasCom for building our gas infrastructure system. We are also grateful for interesting discussions on silane chemistry with Werner Filtvedt and Martin Kirkengen at Cenate.

This work was performed within the two research centers FME Solar United (NFR project no. 193829) and FME SUSOLTECH (NFR project no. 257639), both of which were co-financed by the center partners and the Research Council of Norway. Anjitha S. Geetha is supported by NFR project no. 272393 financed by the Research Council of Norway.

References

[1] G. Cellere, T. Falcon, M. Zwegers, J. Bernreuter, J. Haase, G. Coletti, Int. Technol. Roadmap Photovoltaic 8 (2017) 1–57.
[2] M. Ram, D. Bogdanov, A. Aghanhosseini, S. Oyewo, A. Gulagi, M. Child, C. Breyer, H.-J. Fell, Global Energy System Based on 100% Renewable Energy - Power Sector. Study by Lappeerenranta, University of Technology and Energy Watch Group, 2017.
[3] OECD/IEA, 2018 World Energy Outlook: Executive Summary, 2018. < www.iea.org/t&c/ > (accessed June 18, 2019).
[4] F. Cucchiella, I. D'Adamo, Estimation of the energetic and environmental impacts of a roof-mounted building-integrated photovoltaic systems, Renew. Sustain. Energy Rev. 16 (2012) 5245–5259, https://doi.org/10.1016/j.rser.2012.04.034.
[5] D. Ravikumar, B. Wender, T.P. Seager, M.P. Fraser, M. Tao, A climate rationale for research and development on photovoltaics manufacture, Appl. Energy 189 (2017) 245–256, https://doi.org/10.1016/j.apenergy.2016.12.050.
[6] Z. Nie, P.A. Ramachandran, Y. Hou, Optimization of effective parameters on Siemens reactor to achieve potential maximum deposition radius: an energy consumtion analysis and numerical simulation, Int. J. Heat Mass Transf. 117 (2018) 1083–1098, https://doi.org/10.1016/j.ijheatmasstransfer.2017.10.084.
[7] G. Bye, B. Ceccaroli, Solar grade silicon: technology status and industrial trends, Sol. Energy Mater. Sol. Cells 130 (2014) 634–646, https://doi.org/10.1016/j.solmat.2014.06.019.
[8] A. Ramos, W.O. Filtvedt, D. Lindholm, P.A. Ramachandran, A. Rodríguez, C. del Cañizo, Deposition reactors for solar grade silicon: a comparative thermal analysis of a Siemens reactor and a fluidized bed reactor, J. Cryst. Growth 431 (2015) 1–9, https://doi.org/10.1016/j.jcrysgro.2015.08.023.

[9] S.K. Chunduri, M. Schmela, Market Survey Polysilicon CVD Reactors 2017, Taiang News. (2017) 1–39.

[10] P. Zhang, Effect of operation parameters on fines formation during thermal decomposition of silane, Sol. Energy 155 (2017) 75–81, https://doi.org/10.1016/j.solener.2017.06.019.

[11] W.O. Filtvedt, M. Javidi, A. Holt, M.C. Melaaen, E. Marstein, H. Tathgar, P. Ramachandran, Development of fluidized bed reactors for silicon production, Sol. Energy Mater. Sol. Cells 94 (2010) 1980–1995, https://doi.org/10.1016/j.solmat.2010.07.027.

[12] S.L. Girshick, M.T. Swihart, M.R. Mahajan, S. Nijhawan, Numerical modeling of gas-phase nucleation and particle growth during chemical vapor deposition of silicon, J. Electrochem. Soc. 147 (2000) 2303–2311, https://doi.org/10.1149/1.1393525.

[13] J. Li, G. Chen, P. Zhang, W. Wang, J. Duan, Technical challenges and progress in fluidized bed chemical vapor deposition of polysilicon, Chinese J. Chem. Eng. 19 (2011) 747–753, https://doi.org/10.1016/S1004-9541(11)60052-9.

[14] T.R. Hogness, T.L. Wilson, W.C. Johnson, The thermal decomposition of silane, J. Am. Chem. Soc. 58 (1936) 108–112, https://doi.org/10.1021/ja01292a036.

[15] J.O. Odden, P.K. Egeberg, A. Kjekshus, From, monosilane to crystalline silicon, Part I: Decomposition of monosilane at 690–830K and initial pressures 0.1–6.6MPa in a free-space reactor, Sol. Energy Mater. Sol. Cells. 86 (2005) 165–176, https://doi.org/10.1016/j.solmat.2004.07.002.

[16] A. Onischuk, A. Levykin, V. Strunin, K. Sabelfeld, V. Panfilov, Aggregate formation under homogeneous silane thermal decomposition, J. Aerosol Sci. 31 (2000) 1263–1281, https://doi.org/10.1016/S0021-8502(00)00031-8.

[17] A.A. Onischuk, V.P. Strunin, M.A. Ushakova, V.N. Panfilov, On the pathways of aerosol formation by thermal decomposition of silane, J. Aerosol Sci. 28 (1997) 207–222, https://doi.org/10.1016/S0021-8502(96)00061-4.

[18] F. Slootman, J.-C. Parent, Homogeneous gas-phase nucleation in silane pyrolysis, J. Aerosol Sci. 25 (1994) 15–21, https://doi.org/10.1016/0021-8502(94)90178-3.

[19] Z.M. Qian, H. Michiel, A. Van Ammel, J. Nijs, R. Mertens, Interuniversitair, homogeneous gas phase nucleation of silane in low pressure chemical vapor deposition (LPCVD), J. Electrochem. Soc. Solid-State Sci. Technol. 135 (1988) 2378–2379, https://doi.org/10.1149/1.2096275.

[20] G.M. Wyller, T.J. Preston, H. Klette, Ø. Nordseth, T. Mongstad, W.O. Filtvedt, E.S. Marstein, Critical nucleation concentration for monosilane as function of temperature observed in a free space reactor, Energy Proc. 92 (2016) 904–912, https://doi.org/10.1016/j.egypro.2016.07.100.

[21] G.M. Wyller, T. Preston, T.T. Mongstad, H. Klette, Ø. Nordseth, D. Lindholm, W.O. Filtvedt, E.S. Marstein, Thermal decomposition of monosilane observed in a free space reactor, in: EU PVSEC XXXII 2BO.2.2, Munich, 2016, pp. 294–299.

[22] A. Yuuki, Y. Matsui, K. Tachibana, A numerical study on gaseous reactions in silane pyrolysis, Jpn. J. Appl. Phys. 26 (1987) 747–754.

[23] M.T. Swihart, S.L. Girshick, Thermochemistry and kinetics of silicon hydride cluster formation during thermal decomposition of silane, J. Phys. Chem. B. 103 (1999) 64–76, https://doi.org/10.1021/jp983358e.

[24] S. Nijhawan, P.H. McMurry, M.T. Swihart, S.-M. Suh, S.L. Girshick, S.A. Campbell, J.E. Brockmann, An experimental and numerical study of particle nucleation and growth during low-pressure thermal decomposition of silane, J. Aerosol Sci. 34 (2003) 691–711, https://doi.org/10.1016/S0021-8502(03)00029-6.

[25] W.J. Menz, M. Kraft, A new model for silicon nanoparticle synthesis, Combust. Flame. 160 (2013) 947–958, https://doi.org/10.1016/j.combustflame.2013.01.014.

[26] M. Gröschel, K. Richard, M. Walther, W. Peukert, Process control strategies for the gas phase synthesis of silicon nanoparticles 73 (2012) 181–194. doi:10.1016/j.ces.2012.01.035.

[27] H. Wong, X. Li, M.T. Swihart, L.J. Broadbelt, Detailed kinetic modeling of silicon nanoparticle formation chemistry via automated mechanism generation, J. Phys. Chem. A. 108 (2004) 10122–10132, https://doi.org/10.1021/jp049591w.

[28] A.J. Adamczyk, M.-F. Reyniers, G.B. Marin, L.J. Broadbelt, Kinetic correlations for H2 addition and elimination reaction mechanisms during silicon hydride pyrolysis, Phys. Chem. Chem. Phys. 12 (2010) 12676–12696, https://doi.org/10.1039/c0cp00666a.

[29] A.J. Adamczyk, M.F. Reyniers, G.B. Marin, L.J. Broadbelt, Exploring 1,2-hydrogen shift in silicon nanoparticles: reaction kinetics from quantum chemical calculations and derivation of transition state group additivity database, J. Phys. Chem. A. 113 (2009) 10933–10946, https://doi.org/10.1021/jp9062516.

[30] J.H. Purnell, R. Walsh, The pyrolysis of monosilane, Proc. R. Soc. London, Ser. A. 293 (1966) 543–561, https://doi.org/10.1098/rspa.1966.0189.

[31] G.M. Wyller, T.J. Preston, T.T. Mongstad, D. Lindholm, H. Klette, Ø. Nordseth, W.O. Filtvedt, E.S. Marstein, Influence of temperature and residence time on thermal decomposition of monosilane, Energy Proc. 124 (2017) 812–822, https://doi.org/10.1016/j.egypro.2017.09.352.

[32] C.J. Giunta, R.J. McCurdy, J.D. Chapple-Sokol, R.G. Gordon, Gas-phase kinetics in the atmospheric pressure chemical vapor deposition of silicon from silane and disilane, J. Appl. Phys. 67 (1990) 1062–1075, https://doi.org/10.1063/1.345792.

[33] M. Frenklach, L. Ting, H.W. Ang, M.J. Rabinowitz, Silicon particle formation in pyrolysis of silane and disilane, Isr. J. Chem. 36 (1996) 293–303, https://doi.org/10.1002/ijch.199600041.

[34] A.J. Adamczyk, L.J. Broadbelt, The role of multifunctional kinetics during early-stage silicon hydride pyrolysis: reactivity of Si 2 H 2 isomers with SiH 4 and Si 2 H 6, J. Phys. Chem. A. 115 (2011) 2409–2422, https://doi.org/10.1021/jp1118376.

[35] A.J. Adamczyk, M.-F. Reyniers, G.B. Marin, L.J. Broadbelt, Kinetics of substituted silylene addition and elimination in silicon nanocluster growth captured by group additivity, ChemPhysChem 11 (2010) 1978–1994, https://doi.org/10.1002/cphc.200900836.

[36] S. Vepřek, K. Schopper, O. Ambacher, W. Rieger, M.G.J. Vepřek-Heijman, Mechanism of cluster formation in a clean silane discharge, J. Electrochem. Soc. 140 (1993) 1935–1942, https://doi.org/10.1149/1.2220742.

[37] G.M. Wyller, T.J. Preston, H. Klette, T.T. Mongstad, E.S. Marstein, Identification of higher order silanes during monosilane pyrolysis using gas chromatography-mass spectrometry, J. Cryst. Growth. 498 (2018) 315–327, https://doi.org/10.1016/j.jcrysgro.2018.03.024.

[38] S. Vepřek, M. Heintze, The mechanism of plasma-induced deposition of amorphous silicon from silane, Plasma Chem. Plasma Process. 10 (1990) 3–26, https://doi.org/10.1007/BF01460445.

[39] J.J. Wagner, S. Vepřek, Kinetic study of the heterogeneous Si/H system under low-pressure plasma conditions by means of mass spectrometry, Plasma Chem. Plasma Process. 2 (1982) 95–107, https://doi.org/10.1007/BF00566860.

[40] K. Ensselen, S. Vepřek, Dominant reaction channels and the mechanism of silane decomposition in a H2-Si(s)-SiH4 glow discharge, Plasma Chem. Plasma Process. 7 (1987) 139–153, https://doi.org/10.1007/BF01019174.

[41] P. Ho, M.E. Coltrin, W.G. Breiland, Laser induced fluorecence measuremetns and kinetic analysis of Si atom formation in a rotating disk chemical vapor deposition reactor, J. Phys. Chem. 98 (1994) 10138–10147, https://doi.org/10.1021/j100091a032.

[42] S.S. Talukdar, M.T. Swihart, Aerosol dynamics modeling of silicon nanoparticle formation during silane pyrolysis: a comparison of three solution methods, J. Aerosol. Sci. 35 (2004) 889–908, https://doi.org/10.1016/j.jaerosci.2004.02.004.

[43] H.Y. Dang, M.T. Swihart, Computational modeling of silicon nanoparticle synthesis: I. A general two-dimensional model, Aerosol Sci. Technol. 43 (2009) 250–263, https://doi.org/10.1080/02786820802598059.

[44] H.Y. Dang, M.T. Swihart, Computational modeling of silicon nanoparticle synthesis: II. A two-dimensional bivariate model for silicon nanoparticle synthesis in a laser-driven reactor including finite-rate coalescence, Aerosol Sci. Technol. 43 (2009) 554–569, https://doi.org/10.1080/02786820902790325.

[45] A.J. Adamczyk, M.F. Reyniers, G.B. Marin, L.J. Broadbelt, Hydrogenated amorphous silicon nanostructures: novel structure-reactivity relationships for cyclization and ring opening in the gas phase, Theor. Chem. Acc. 128 (2011) 91–113, https://doi.org/10.1007/s00214-010-0767-x.

[46] S. Liu, W. Xiao, CFD – PBM coupled simulation of silicon CVD growth in a fl uidized bed reactor: effect of silane pyrolysis kinetic models, Chem. Eng. Sci. 127 (2015) 84–94, https://doi.org/10.1016/j.ces.2015.01.026.

[47] S.-S. Liu, W.-D. Xiao, Numerical simulations of particle growth in a silicon-CVD fluidized bed reactor via a CFD–PBM coupled model, Chem. Eng. Sci. 111 (2014) 112–125, https://doi.org/10.1016/j.ces.2014.02.021.

[48] F.C. Eversteijn, Gas-phase Decomposition of silane in a horizontal epitaxial reactor, Philips Res. Repts. 26 (1971) 134–144.

[49] R. Körmer, M.P.M. Jank, H. Ryssel, H.-J. Schmid, W. Peukert, Aerosol synthesis of silicon nanoparticles with narrow size distribution—Part 1: Experimental investigations, J. Aerosol Sci. 41 (2010) 998–1007, https://doi.org/10.1016/j.jaerosci.2010.05.007.

[50] R. Körmer, H.-J. Schmid, W. Peukert, Aerosol synthesis of silicon nanoparticles with narrow size distribution—Part 2: Theoretical analysis of the formation mechanism, J. Aerosol Sci. 41 (2010) 1008–1019, https://doi.org/10.1016/j.jaerosci.2010.08.002.

[51] J.O. Odden, P.K. Egeberg, A. Kjekshus, From monosilane to crystalline silicon, part II: Kinetic considerations on thermal decomposition of pressurized monosilane, Int. J. Chem. Kinet. 38 (2006) 309–321, https://doi.org/10.1002/kin.20164.

[52] J.J. Wu, R.C. Flagan, Onset of runaway nucleation in aerosol reactors, J. Appl. Phys. 61 (1987) 1365–1371, https://doi.org/10.1063/1.338115.

[53] G.M. Wyller, T.J. Preston, M.O. Skare, H. Klette, S.G. Anjitha, E.S. Marstein, Exploring thermal pyrolysis of monosilane through gas chromatography-mass spectrometry measurements of higher order silanes, Silicon Chem. Sol. Ind., Svolvær (2018) 267–275.

[54] M.S.D.C. NIST, S.E. Stein, Mass Spectra, in: NIST Chem. WebBook, NIST Stand. Ref. Database Number 69, Eds. P.J. Linstrom W.G. Mallard, National Institute of Standards and Technology, Gaithersburg MD, 2018. doi: 10.18434/T4D303, (retrieved February 1, 2018).

[55] Y.-K. Kim, K.K. Irikura, M.E. Rudd, M.A. Ali, M. Stone, Electron-Impact Cross Sections for Ionization and Excitation Database, in: NIST Chem. WebBook, NIST Stand. Ref. Database Number 69, Eds. P.J. Linstrom W.G. Mallard, NIST Physical Measurement Laboratory, 2018. < https://www.nist.gov/pml/electron-impact-cross-sections-ionization-and-excitation-database > (retrieved February 1, 2018).

[56] J. Simon, R. Feurer, A. Reynes, R. Morancho, Thermal dissociation of disilane: quadrupole spectrometry investigation, J. Anal. Appl. Pyrolysis. 24 (1992) 51–59, https://doi.org/10.1016/0165-2370(92)80004-6.

[57] K. Tonokura, T. Murasaki, M. Koshi, Formation mechanism of hydrogenated silicon clusters during thermal decomposition of disilane, J. Phys. Chem. B. 106 (2002) 555–563, https://doi.org/10.1021/jp015523n.